ChemComm

Structural studies of perovskite $La_{1-x}Sr_xCoO_{3-\delta}$ during chemical looping with methane

Journal:	*ChemComm*
Manuscript ID	CC-COM-12-2018-009573.R1
Article Type:	Communication

Journal Name

COMMUNICATION

Received 00th January 20xx,
Accepted 00th January 20xx

DOI: 10.1039/x0xx00000x

www.rsc.org/

Structural studies of perovskite $La_{1-x}Sr_xCoO_{3-\delta}$ during chemical looping with methane †

Tianyu Li [a], Rishvi S. Jayathilake [a], Daniel D. Taylor [b] and Efrain E. Rodriguez [a]*

Perovskite oxides are promising materials as oxygen carriers in chemical looping applications. We analyze *in situ* X-ray diffraction data on the perovskite phases $La_{1-x}Sr_xCoO_{3-\delta}$ for *x*=0, 0.25, 0.5, and 0.75 under chemical looping conditions. We report and discuss their structural evolution, cycling stability, and suitability as oxygen strorage materials.

The efficient use of fuels such as natural gas remains an outstanding challenge. Chemical looping reactions offer a potential solution since they are reversible, thermochemical processes that can be applied in fuel combustion and reforming.[1] In a typical chemical looping reactor, an oxygen storage material (OSM) alternately releases its lattice oxygen to oxidize fuels and then reuptakes oxygen from air into its lattice, thus completing one cycle. Upon oxidation by an OSM, a hydrocarbon fuel such as methane can provide either energy or useful products such as syngas (H_2 + CO). Since OSMs provide a pure oxygen stream in the reactor, the chemical looping reaction affords two promising advantages over conventional combustion or reforming: (1) it prevents formation of NO_x gas and (2) eliminates costly separation of the products from N_2 gas streams.[2,3] The attributes of an ideal OSM include high oxygen storage capacity, fast reaction kinetics, sufficient oxygen anion transport (bulk to surface), and excellent thermal and mechanical stability for cycling at high temperatures. [3,4]

Among known OSMs, ABO_3 perovskite-type oxides (where *A* and *B* are typically metal cations) display several of the attributes mentioned above for chemical looping. Principally, perovskites can display fast reaction kinetics and long term structural and mechanical stability at elevated temperatures. [1] A significant feature of ABO_3 perovskites as OSMs is that both the *A* and *B* metals can be modified to further improve their performance in chemical looping reactions.[5,6,7] Few studies have really focused on the cycling stability of the OSMs, which is relevant if we want to find an OSM that will function effectively in a chemical looping reactor.

Our previous studies show that *in situ* synchrotron X-ray powder diffraction (SXRD) is a powerful tool to study reaction kinetics and cycling stability of OSMs under chemical looping conditions. [8, 6] At the same time, we can follow the structural evolution of OSMs during the entire cycles. Previous studies demonstrated that the perovskite $LaCoO_3$ displayed high oxygen storage capacity [7] as well as product selectivity toward oxidation of methane.[9,10] We therefore decided to study the series $La_{1-x}Sr_xCoO_{3-\delta}$ with *in situ* SXRD to reveal its cycling stability and structural evolution during chemical looping. We performed all SXRD experiments on the 17-BM beamline at the Advanced Photon Source (APS) at Argonne National Laboratory. We prepared a series of perovskite type $La_{1-x}Sr_xCoO_{3-\delta}$ phases for x = 0, 0.25, 0.5, 0.75 using syntheses reported previously.[10] Details on the syntheses are provided in the electronic supplementary information file.† The x = 1 member was not included in this study since the perovskite phase of $SrCoO_{3-\delta}$ is not stable under ambient oxygen partial pressures.[11] We characterized each sample with SXRD at room temperature, and subsequently performed Rietveld refinement using TOPAS 4.[12] The structural fits and results are presented in Figures S1-S5. All samples except $LaCoO_{3-\delta}$ contain a small amount of impurity (5 wt. % to 8 wt. % of $LaSrCoO_4$). We obtained the values for x from Rietveld refinement of the metal occupancies (**Table S1-S4**). Within the standard uncertainty (s.u.) of those refinements, the values of x are close to the nominal values stated above, and the occupancy of Co is also close to unity.

[a] *Department of Chemistry and Biochemistry, University of Maryland, College Park, Maryland 20742-2115, USA. E-mail: efrain@umd.edu*
[b] *Department of Materials Science and Engineering, University of Maryland, College Park, Maryland, 20742-2115, USA*
† *Electronic Supplementary Information (ESI) available: [details of any supplementary information available should be included here]. See DOI: 10.1039/x0xx00000x*

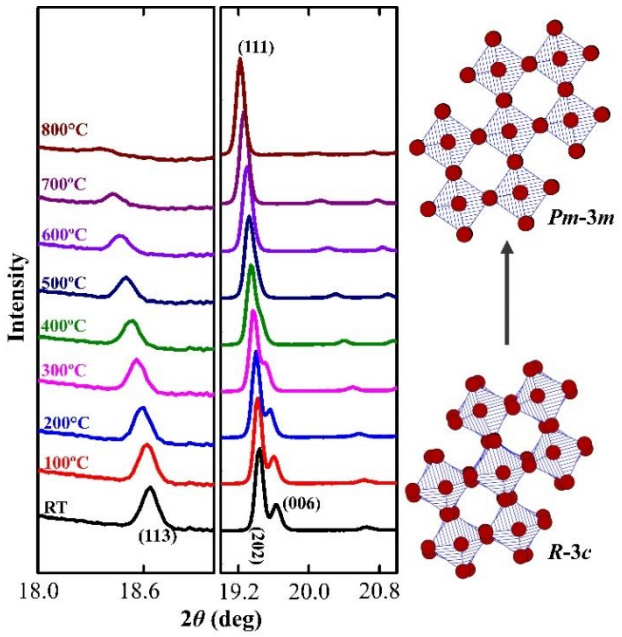

Fig.1 *In situ* SXRD patterns (λ=0.75009 Å) of $La_{0.75}Sr_{0.25}CoO_{3-\delta}$ under air flow from room temperature (RT) to 800 °C. The diffraction patterns indicate the gradual phase transition of $La_{0.75}Sr_{0.25}CoO_{3-\delta}$ upon heating. The panel on the left shows the disappearance of the (113) peak while the panel on the right shows the merging of two peaks in the trigonal $R\bar{3}c$ phase in to a single peak in the cubic $Pm\bar{3}m$ phase.

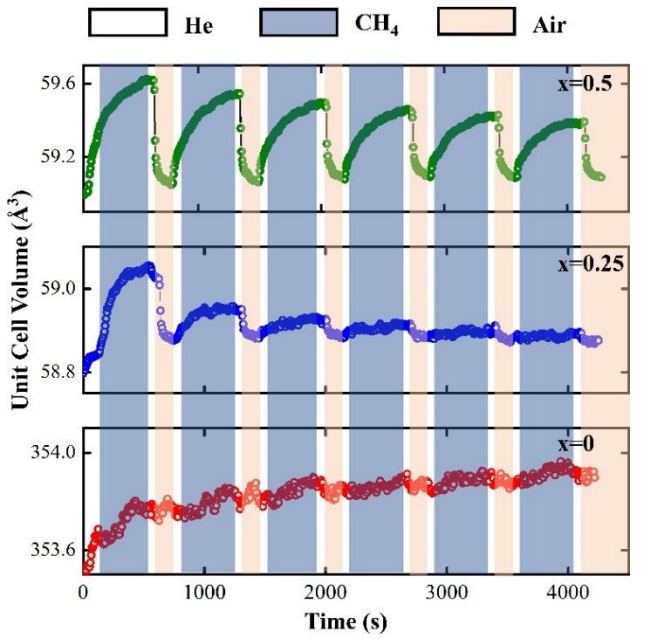

Fig.2 Refined unit cell volume from *in situ* SXRD (λ=0.75009Å) measurements on $La_{1-x}Sr_xCoO_{3-\delta}$ for x = 0, 0.25, and 0.5. Six chemical looping cycles were performed at 800 °C. For the x = 0, the patterns are refined with $R\bar{3}c$ symmetry. For the x=0.25 and 0.5 samples, the patterns are refined with $Pm\bar{3}m$ symmetry.

At room temperature $La_{1-x}Sr_xCoO_{3-\delta}$ for x = 0, 0.25, and 0.5 adopts the trigonal $R\bar{3}c$ space group. The powder diffraction peak corresponding to the (113) Bragg reflection at a 2ϑ of approximately 18.7° is characteristic of the trigonal phase since the primitive cubic phase lacks this reflection (Figure S4). However, the x=0.75 member adopts the cubic space group $Pm\bar{3}m$ at room temperature. The higher Sr content increases the symmetry of the perovskite structure since the tolerance factor approaches unity. [13,14]

Next, we heated the entire series of oxides to 800 °C from room temperature under air flow while measuring their diffraction patterns. We collected *in situ* SXRD patterns every 6.5 seconds. Upon heating, the crystal structures of the four samples evolved distinctly. The evolution of the diffraction patterns from room temperature to 800 °C are presented in Figure S6. We focus on the most important features of the ramping study.

First, $LaCoO_3$ retains the trigonal $R\bar{3}c$ structure throughout the temperature range and only expands its lattice volume linearly (Figure S6a). Second, the $La_{0.75}Sr_{0.25}CoO_{3-\delta}$ sample undergoes a trigonal $R\bar{3}c$ to cubic $Pm\bar{3}m$ phase transition as shown in **Figure 1**. The phase transition is marked by the merging of the (111) and (006) reflections and concomitant disappearance of the (113) reflection. This gradual phase transition appears to be complete by 800°C. For the samples with a higher level of Sr substitution, the phase transition is complete at lower temperatures. For the x = 0.5 sample, we observed the transition occurs around 300 °C (Figure S6c). For the x = 0.75 sample, we observed it to remain cubic for the entire temperature range (Figure S3d). These phase transition behavior of $La_{1-x}Sr_xCoO_{3-\delta}$ broadly reproduces the results of Mastin et al.[13] One key difference between our studies., is that we found the phase transition in $La_{0.5}Sr_{0.5}CoO_{3-\delta}$ to not reach completion until 300 °C whereas they found it at 200 °C.[13]

In our third experiment, we simulated the conditions within a chemical-looping reactor while taking diffraction patterns. We held the samples at a fixed temperature while the atmosphere was cycled between 20% Air/He and 15% CH_4/He. In between each gas change, we used 100% He to purge the atmosphere. As illustrated in Figure S9, the main phases of the $La_{1-x}Sr_xCoO_{3-\delta}$ (x = 0, 0.25, 0.5) samples retained their crystal structures under both atmospheres at 800 °C ($R\bar{3}c$ for x = 0 and $Pm\bar{3}m$ for x = 0.25, 0.5). To monitor the oxygen release and uptake of the perovskites, we analyzed the unit cell volume as a function of time. To this end, we performed Rietveld refinement on each diffraction pattern to extract unit cell volumes. The change of unit cell volume for $La_{1-x}Sr_xCoO_{3-\delta}$ (x = 0, 0.25, 0.5) under the chemical looping cycles is plotted in **Figure 2**.

We next explain the significance of the volume change for chemical looping. As the metal oxide is reduced in a methane atmosphere, it releases its lattice oxygen. The loss of oxide anions in the lattice increases the ionic and repulsive forces between cations. Thus, the loss of oxygen expands the unit cell volume in the perovskite oxide.[15] The oxidizing atmosphere drives oxygen back into the crystal lattice causing the opposite effect of shrinking the unit cell. **Figure 2** shows that within one cycle, the x = 0.5 analogue underwent a faster unit cell volume change than the x = 0 and 0.25 samples. All the samples underwent the same ball milling procedure, and we did not observe significant differences in particle size from Scanning Electron Microscopy (SEM) (Figure S10). We therefore conclude

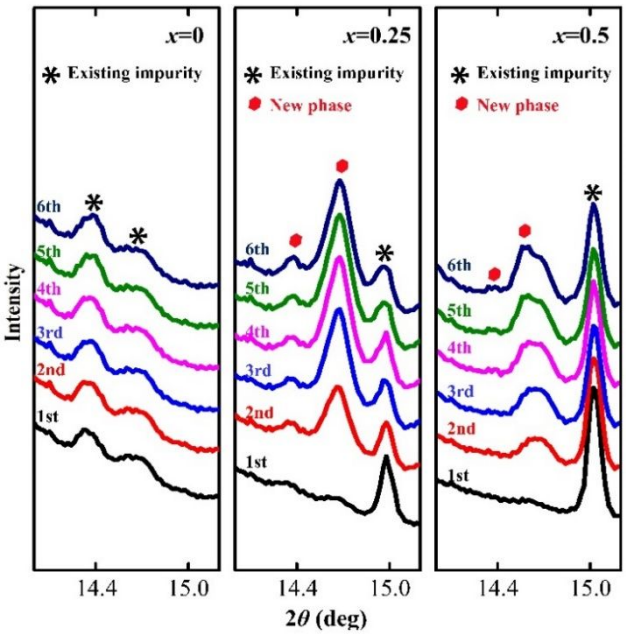

Fig.3 Comparison of SXRD diffraction patterns at the end of each chemical looping cycle (under air) for the x=0, 0.25, 0.5 members of $La_{1-x}Sr_xCoO_{3-\delta}$. The number above each curve represents sequence number from cycling. For the x=0.25 and x=0.5 samples, the appearance of new peaks upon cycling indicates decomposition of the perovskite phase. The existing impurity in the x=0.25 and x=0.5 samples is $LaSrCoO_4$.

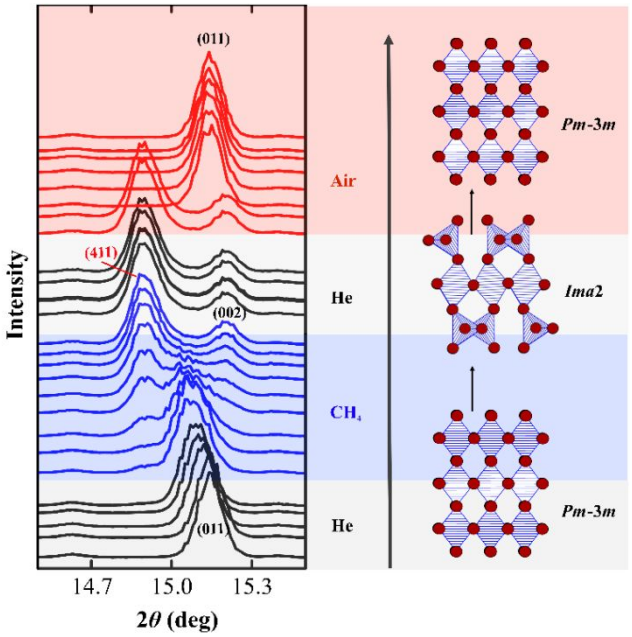

Fig.4 Time evolution of *in situ* SXRD patterns (λ=0.72768 Å) of $La_{0.25}Sr_{0.75}CoO_{3-\delta}$ under He/CH_4/air atmospheres within one chemical looping cycle at 700 °C. The structural evolution corresponding to the changes in the powder diffraction patterns is depicted on the right.

that particle size does not play a major role in differentiating the kinetics between samples.

The improved kinetics for cycling with increasing Sr substitution can be explained by the increase of oxide anion conductivity.[16] As the trivalent La^{3+} is substituted by the divalent Sr^{2+}, oxygen vacancies are introduced to achieve charge balance. Higher levels of oxygen vacancies therefore benefit the transport of O^{2-} within the crystal lattice, leading to faster reaction rates. With more oxygen vacancies, the repulsive forces between the cations are also greater. **Figure 2** also shows that the unit cell volume change is greater as the Sr content is increased. Indeed, $LaCoO_3$ displays a negligible change in unit cell volume. Therefore, just as we previously observed with $LaFeO_3$,[6] the x=0 member in this series displays either slow kinetics or nonreactivity with air and methane at 800 °C.The periodic change of unit cell volume for the x = 0.25 and 0.5 samples indicates that they can be successfully cycled with methane and air. However, **Figure 2** shows that their unit cell volumes never fully recover to their initial state at the end of subsequent cycles. With each cycle the change in unit cell volume decreases, which indicates a degradation of chemical looping performance. A closer look at the diffraction patterns at the end of each cycle reveals the possible reason for this degradation. First, we monitored any change in the crystallite size by plotting the broadening parameter from the Rietveld fits as a function of cycle. We found no change in crystallite size upon cycling within error (Figure S11) and conclude that significant degradation of crystallinity does not occur. Second, we looked for possible new phases during cycling and found new, weak reflections. **Figure 3** shows selected region of SXRD patterns at the end of each cycling. Two peaks (2θ around 14.4° and 14.7°) appear after several cycles for the x = 0.25 and 0.5 members, which are likely related to degradation during cycling. In $LaCoO_3$, those two peaks exist as an impurity in the initial material and remain constant even after several cycles. Contrastingly, for the Sr-substituted samples, those two peaks grow in intensity after each cycle. Therefore, while Sr substitution and introduction of oxide anion vacancies lead to increased reactivity for chemical looping, it also destabilizes the perovskite towards this unknown phase. Due to the low intensity of the impurity peaks and possible peak overlap, we could not identify the unknown phase. A similar decomposition of $La_{1-x}Sr_xCoO_{3-\delta}$ at low oxygen partial pressures has been previously reported.[14]

To study whether lower temperatures can improve looping performance by impeding degradation, two cycles were performed for $La_{0.5}Sr_{0.5}CoO_{3-\delta}$ at 700 °C. As previously done, we extracted the lattice volume changes as a function of time and present the results in Figure S12. At temperatures of 600 °C and 700 °C, the decay is still visible even after 2 cycles, implying decomposition remains at lower temperatures. Meanwhile, the kinetics are too slow at 500 °C for perovskite $La_{0.5}Sr_{0.5}CoO_{3-\delta}$ to function in chemical looping.

We discuss $La_{1-x}Sr_xCoO_{3-\delta}$ (x = 0.75) separately since its chemical looping behaviour is significantly different from the rest of the series. Two chemical looping cycles were performed for $La_{0.25}Sr_{0.75}CoO_{3-\delta}$ at 500 °C, 600 °C, and 700 °C. As depicted in Figure 4, $La_{0.25}Sr_{0.75}CoO_{3-\delta}$ undergoes a gradual phase transition at 700 °C from cubic $Pm\bar{3}m$ perovskite to the brownmillerite *Ima*2 structure under the reducing atmosphere. It then immediately reverts to cubic $Pm\bar{3}m$ once exposed to air. Brownmillerite is related to the perovskite phase except that the Co cations exist in multiple coordination environments since

the oxide vacancies become ordered. We observed a reversible phase transition in the x=0.75 sample since it arises from a transition of order to disorder in the oxygen sublattice. Within the series the x=0.75 sample has the highest concentration of oxide vacancies and is therefore the most sensitive towards changes from oxygen substoichiometry. Two looping cycles were also performed at 500 ℃ and 600 ℃, and the diffraction patterns are presented in Figure S13. No phase transition was observed at 500 ℃, while the transition from cubic perovskite to brownmillerite remained incomplete at 600 ℃. In the case of $SrFeO_{3-\delta}$ from our previous cycling studies,[6] the brownmillerite phase appears to be stabilized when the value of δ is close to 0.5. Even though we do not have neutron diffraction data for the *x*=0.75 sample, it is likely that a similar concentration of oxide vacancies as in $SrFeO_{2.5}$ drives the phase transition.

We now compare the findings between our previous chemical looping study[6] of $La_{1-x}Sr_xFeO_{3-\delta}$ with the present one. First, the chemical stability of the iron analogues appears to be superior to that of the cobalt-based series since the latter's perovskite structure degrades faster under chemical looping conditions.[6] The thermal stability of perovskites is influenced by both the *A* site and *B* sites elements. Since we kept the *A*-site cations constant between the two studies, our observation is likely due to the transition metal (or *B* site). The differences between the ionic radii of Co^{2+}/Co^{3+} and Fe^{2+}/Fe^{3+} are not significant, so we attribute the change in performance between their respective perovskites as OSMs to be an electronic effect. For a given Sr^{2+}:La^{3+} ratio, it appears that the oxidation and reduction of Co within the perovskite structure is less stable than that of Fe. A computational study comparing $LaCoO_3$ to $LaFeO_3$ sheds more light on their difference.[17] This study found that the free energy of formation is less negative for $LaCoO_3$ than it is for $LaFeO_3$. The free energy differences suggest that likewise for the Sr-substituted series, the Co analogues more easily decompose than the Fe ones for similar thermodynamic conditions.

In conclusion, we find that performing *in situ* structural studies of the perovskite series $La_{1-x}Sr_xCoO_{3-\delta}$ is a powerful tool towards understanding its performance for chemical looping with methane. The level of Sr substitution influences the number of oxygen vacancies in the perovskite lattice and therefore leads to observable differences in the crystal structure during both ramping in air and isothermal chemical looping. The more Sr that substitutes for La, the faster the kinetics for oxidation of methane and uptake of oxygen from air. We reaffirm the significance of aliovalent substitution towards improving the kinetics of chemical looping reactions. Although previous studies show perovskite $La_{1-x}Sr_xCoO_{3-\delta}$ to display high oxygen storage capacity[7] and improved product selectivity,[9,10] our *in situ* diffraction study indicates that its performance decays upon subsequent cycles. A possible solution that preserves the fast kinetics of the Co-system yet introduces stability from the Fe-based one would include a solid solution between the two. Therefore, doping $La_{1-x}Sr_xCoO_{3-\delta}$ with Fe on the Co site where *x* is close to 0.5 may lead to an oxide perovskite ideally suited for chemical looping applications. Finally, given how much information one can obtain on the cycling stability and kinetics of OSMs, we propose that *in situ* SXRD studies become more common when investigating OSMs for reactions with hydrocarbon fuels such as methane.

Conflicts of interest

There are no conflicts to declare.

Acknowledgement

We acknowledge the Department of Commerce/NIST award 70NANB12H238 for support. Use of the Advanced Photon Source at Argonne National Laboratory was supported by the U.S. Department of Energy, Office of Science, Office of Basic Energy Sciences, under Contract No. DE-AC02-06CH11357. We thank W. Xu and A. Yakovenko at 17 BM, ANL for their help with SXRD data collection

References

1 X. Zhu, K. Li, L. Neal and F. Li, *ACS Catal.*, 2018, **8**, 8213–8236.

2 L. Liu and M. R. Zachariah, *Energy & Fuels*, 2013, **27**, 4977–4983.

3 J. Adanez, A. Abad, F. Garcia-Labiano, P. Gayan and L. F. de Diego, *Prog. Energy Combust. Sci.*, 2012, **38**, 215–282.

4 J. Adánez, L. F. de Diego, F. García-Labiano, P. Gayán, A. Abad and J. M. Palacios, *Energy & Fuels*, 2004, **18**, 371–377.

5 A. Evdou, V. Zaspalis and L. Nalbandian, *Fuel*, 2010, **89**, 1265–1273.

6 D. D. Taylor, N. J. Schreiber, B. D. Levitas, W. Xu, P. S. Whitfield and E. E. Rodriguez, *Chem. Mater.*, 2016, **28**, 3951–3960.

7 L. Liu, D. D. Taylor, E. E. Rodriguez and M. R. Zachariah, *Chem. Commun.*, 2016, **52**, 10369–10372.

8 R. Jayathilake, B. Levitas and E. E. Rodriguez, *J. Mater. Chem. A*, 2018, **6**, 4801–4810.

9 K. Zhao, F. He, Z. Huang, G. Wei, A. Zheng, H. Li and Z. Zhao, *Appl. Energy*, 2016, **168**, 193–203.

10 K. T. C. Roseno, R. Brackmann, M. A. da Silva and M. Schmal, *Int. J. Hydrogen Energy*, 2016, **41**, 18178–18192.

11 H. Jeen, W. S. Choi, J. W. Freeland, H. Ohta, C. U. Jung and H. N. Lee, *Adv. Mater.*, 2013, **25**, 3651–3656.

12 B. Y. R. W. Cheary and A. Coelho, *J. Appl. Cryst.*, 1992, **25**, 109–121.

13 J. Mastin, M. A. Einarsrud and T. Grande, *Chem. Mater.*, 2006, **18**, 6047–6053.

14 J. Ovenstone, J. S. White and S. T. Misture, *J. Power Sources*, 2008, **181**, 56–61.

15 D. Marrocchelli, N. H. Perry and S. R. Bishop, *Phys. Chem. Chem. Phys.*, 2015, **17**, 10028–10039.

16 A. B. Muñoz-García, A. M. Ritzmann, M. Pavone, J. A. Keith and E. A. Carter, *Acc. Chem. Res.*, 2014, **47**, 3340–3348.

17 F. Calle-Vallejo, J. I. Martínez, J. M. García-Lastra, M. Mogensen and J. Rossmeisl, *Angew. Chemie Int. Ed.*, 2010, **49**, 7699–7701.

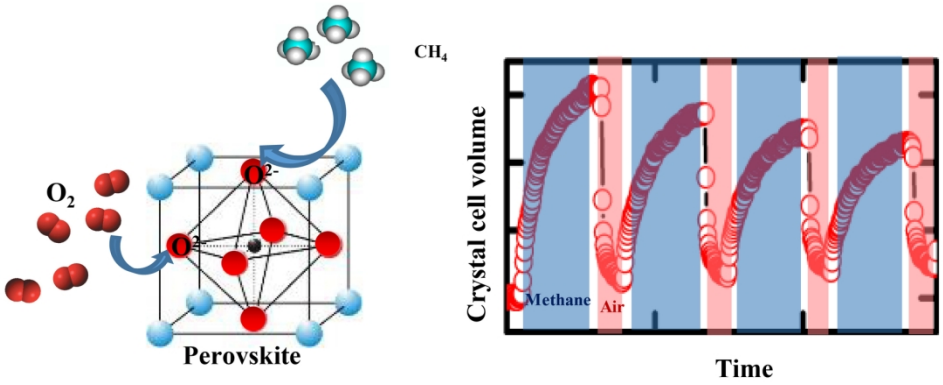

Perovskite oxides for chemical looping of methane

80x40mm (600 x 600 DPI)